Engineered Science
DOI: https://dx.doi.org/10.30919/es1432

Analysis of Heat Transfer and Flow Behaviors of Magnetic Fluid in Twisted Square Tubes with Alternating Electromagnetic Fields

Jarinee Jongpluempiti,[1] Ponthep Vengsungnle,[1] Sahassawas Poojeera,[2] Nittaya Naphon,[3] Smith Eiamsa-ard[4] and Paisarn Naphon[5,*]

Abstract

This work investigated the thermal and flow behaviors of magnetic fluid flowing in the twisted square tubes with various twisted pitches, both with and without an electromagnetic field (EF) influence. The Reynolds number ranged from 4500 to 10500, with a pitch spacing of 100-200 mm, power input of 180-220 V, electromagnetic flux of 0.25-6.5 μT, frequency of 0.25-1.25 Hz, and nanofluid concentration of 0.02% by vol. Without EF, the twisted square tube has a more significant Nusselt number and flow resistance than the straight square tube, and the magnetic fluid increases by 10.5% and 5.35%, respectively. The electromagnetic field causes particles to migrate toward the square tube wall, which significantly influences boundary layer disturbance. Increased electromagnetic flux and frequency increase the intensity of nanoparticle turbulence and the coolant thermal conductivity. The EF flux effect increases the Nusselt number by 10.71% and the friction factor by 5.78%. In addition to the EF frequency effect, the Nusselt number increases by 13.45%. Furthermore, the predicted results are generally compatible with the observed data, with a maximum error of 7.92%.

Keywords: Twisted square tube; Numerical analysis; Electromagnetic field; Magnetic-fluid.
Received: 13 January 2025; Revised: 05 February 2025; Accepted: 17 February 2025.
Article type: Research article.

1. Introduction

Traditional heat transfer applications, , particularly cooling procedures, have used fluids, including water, oil, and ethylene glycol, as their principal working medium. However, the limits of thermal physical properties may result in slower heat transfer rates and thus a reduced cooling system efficacy. Introducing particles of nanoscale size into ordinary fluids is a viable method of bypassing this constraint. These nanoparticles significantly enhance the thermal properties and raise the heat transfer capabilities. Choosing suitable nanoparticles among enormous number of nanoparticles available is critical. This choice is based on the nanoparticle's inherent thermophysical characteristics. These variables must be carefully considered when selecting a nanoparticle for cooling techniques. Ferrofluids are colloidal suspensions made up of the based fluid and nanoparticles. They seem to be helpful in thermal processes and other practice areas. Ferrofluids may drastically affect the flow behavior of the magnetic field (MF). Furthermore, in some areas, the magnetic force from the external MF can give to the ferrofluid. Ferrofluid has been employed in various applications across several scientific disciplines.[1]

Furthermore, an artificial neural network (ANN) was applied in the analysis of nanofluids in mini-channel,[2,3] spiral-coil tube heat exchangers,[4,5] micro-channel heat sink units,[6] and three-start helical fluted tubes.[7] The next step was examining how binary magnetic liquid thermal cooling increased with a MF.[8,9] Salehi *et al*.[10] considered the efficiency of a thermosyphon with the MF, and the Lorentz

[1] *Department of Agricultural Machinery Engineering, Faculty of Engineering and Architecture, Rajamangala University of Technology Isan, Nakhonratchasima 30000, Thailand*
[2] *Department of Mechanical Engineering, Faculty of Engineering, Rajamangala University of Technology Isan, Khon Kaen Campus, 40000, Thailand*
[3] *Department of Pharmaceutical Chemistry, Faculty of Pharmacy, Srinakharinwirot University, 63 Rangsit-Nakhornnayok Rd., Ongkharak, Nakhorn-Nayok, 26120, Thailand*
[4] *Department of Mechanical Engineering, Faculty of Engineering, Mahanakorn University of Technology, Bangkok, 10530, Thailand*
[5] *Department of Mechanical Engineering, Faculty of Engineering, Srinakharinwirot University, 63 Rangsit-Nakhornnayok Rd., Ongkharak, Nakhorn-Nayok, 26120, Thailand*
**Email:* paisarnn@g.swu.ac.th (P. Naphon)

force enables specialized applications,[11] in which this force is produced by the MF.[12] Furthermore, ferrofluid applications have grown significantly with the increased interest in small heat transfer devices for mini-systems. Tangthieng *et al*.[13] used statistical approaches to investigate the ferrofluid flow in two flat plates. Tzirtzilakis *et al*.[14] considered the magnetic fluids flowing through the rectangular tube. A nonconductor biomagnetic fluid was analyzed using the MF. The mixture model is used to evaluate the ferrofluid heat transfer inside a cylindrical form,[15] a rectangular vertical conduit,[16] and a cylindrical annulus mold.[17] Lajvardi *et al*.[18] examined the ferrofluid heat transport under the MF and in a vertical double tube.[19] Mahian *et al*.[20] studied the magneto-hydrodynamics effect on the heat and flow behaviors flowing in two spinning cylinders.

Ghofrani *et al*.[21] studied the convective heat transport of magnetic fluids using MFs. Rashidi *et al*.[22] used computational methods to consider the velocity and temperature distributions in the rotating disk with MF. Mojumder *et al*.[23] calculated the heat transfer characteristics of ferrofluid (Fe_3O_4/water) in a half-moon-shaped cavity. Sha *et al*.[24] found that MFs altered the cooling efficiency of nanofluids. Gui *et al*.[25] studied using single-phase coolants with a MF to enhance microchannel efficiency. Shi *et al*.[26] considered the thermal behavior of Fe_3O_4 flowing in the tube with MF. Naphon and Wiriyasartmerged two heat transfer enhancement approaches for thermal efficiency,[27] taking into account pulsed flow, MFs, nanofluids, and fluted tubes. Han *et al*.[28] investigated the steel flow characteristics and the corrugated sheet topologies under MFs.[29] Naphon *et al*.[30] considered the heat removal ability of pulsed ferrofluid flow in a fluted tube, and the effects of MF on natural nanofluid heat transfer were considered.[31] Siricharoenpanitch *et al*.[32] examined how nanofluid flow characteristics such as pulsed flow, nanofluid concentration, corrugated tube morphologies, and heat flux influenced MF cooling performance. Nanofluids have been investigated for the hydrothermal efficiency of different channels with a turbulator insert and thermal devices.[33,34] Arunkumar *et al*.[35] considered the thermal efficiency of an absorber tube with different shaped perforation holes. El-Shafay *et al*.[36] used the computational fluid dynamic (CFD) to consider the flow of a magnetic fluid via a heat exchanger tube. Vengsungnle *et al*.[37] considered the impact of a MF on the Nusselt number and pressure drop of ferrofluid in the fluted tubes.

The usefulness of nanofluids in various heat transfer devices and application systems was extensively investigated. According to the previously reviewed process, substantial research has been undertaken on the MF. Several experiments used MFs and nanofluids. Nonetheless, there has been little

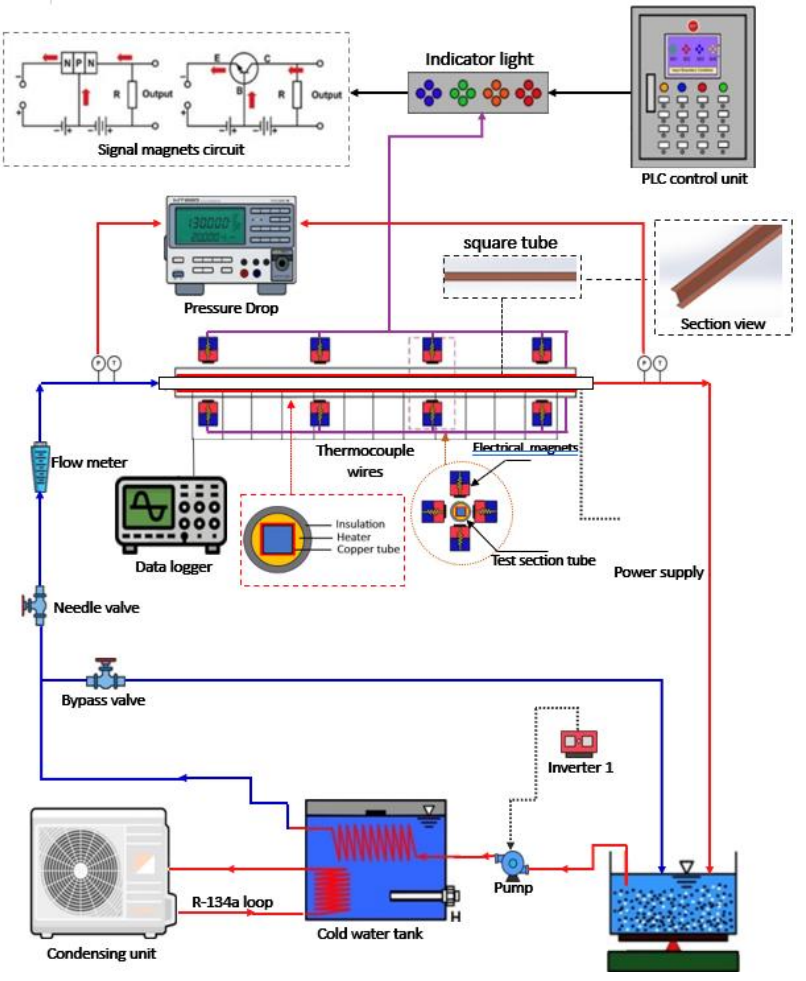

Fig. 1: Schematic diagram of experimental apparatus.

study on linked heat transfer augmentation schemes, namely the oscillation of an electromagnetic field (EF). Thus, this research aims to consider the heat and flow characteristics of ferrofluid in the twisted square tube with and without an EF. Effects of the EF 's frequency, flux, and twisted pitch distance on the temperature and flow behaviors have been considered. To ensure verification, acquired data is matched to previously available data.

2. Experimental

2.1 Experimental system

As shown in Fig. 1, the system was created and built to examine heat removal performance in square tubes with and without a MF. A weight-with-stop watch keeps track of the coolant flow rate, while a pressure transducer measures the Δp throughout the test section. The experiment had four configurations (10×10 mm and 2000 mm). The heat source is a nickel-chromium heater wrapped around a square tube and insulated with an Aeroflex tube. Five thermocouples for coolant and five external surfaces were tested inside the square tube to determine temperature fluctuation. A conventional dry box temperature calibrator is used to calibrate all thermocouples. As soon as the system stabilizes, the DT85 data taker and computer unit—both components of the data collection system—collect the necessary information. The EF system consists of four stations: an electromagnetic system, a PLC system, and a monitored light bulb system. As shown in Fig. 2, each station's electromagnetic system comprises four electric units that operate individually. The circulating coolant in the system is Fe_3O_4/water ferrofluid, which may be combined with a pH eight agent via an ultrasonic device. The nanoparticles have a purity of 99.0%, (spherical shape with 23 nm diameter, from US Research Nanomaterials, Inc.).

2.2 Nanofluid preparation

Ultrasonic mixing achieves a pH of 8 by dispersing Fe_3O_4 nanoparticles (Purity>99.9%) in the base fluid and adding the PH agent (NaOH, from MERCK). This study's use of Fe_3O_4 nanoparticles with thermophysical properties (Table 1) stems from their exceptional reactivity to EFs. The sonicated unit stimulated the nanofluid for 10 minutes on an hour to keep the nanofluid stable. Beyond that, on day one and day two, the UV-1800 spectrophotometer measures the % absorption spectra of the fluid. With decreased sedimentation of nanoparticles, the percentage absorbance spectra on the first and second days were equal, showing that it is still stable. The error was 1.03%.

2.3 Experimental procedure

The experiment had magnetic fluid flowing through the apparatus and a constant inlet temperature of 30°C. The experimental approach examined various coolant flow rates, power input, EF frequency, EF flux, and twisted pitch. Given the required circumstances, the working fluid flow rate gradually increases. A PLC system adjusts the power given to all units and stations to account for the effect of electromagnetic flux. To account for the influence of electromagnetic frequency, each electromagnet unit (all units and stations) must have the same connecting/disconnecting time as shown in Fig. 3. To replicate the experimental findings, the relevant parameters are assessed five times. The Gauss meter (HT201 Gauss meter) measures the average electromagnetic flux of each station.

Table 1: Thermophysical properties of water, Fe_3O_4 (25 °C).

Properties	Fe_3O_4
Density, ρ (kg ·m^{-3})	5180
Thermal conductivity, k (W·m^{-1}·K^{-1})	80.4
Viscosity, μ (m·Pa·S)	-
Specific heat, C_p (J·kg^{-1}·K^{-1})	670
Purity (%)	>99.9
Average diameter (nm)	23

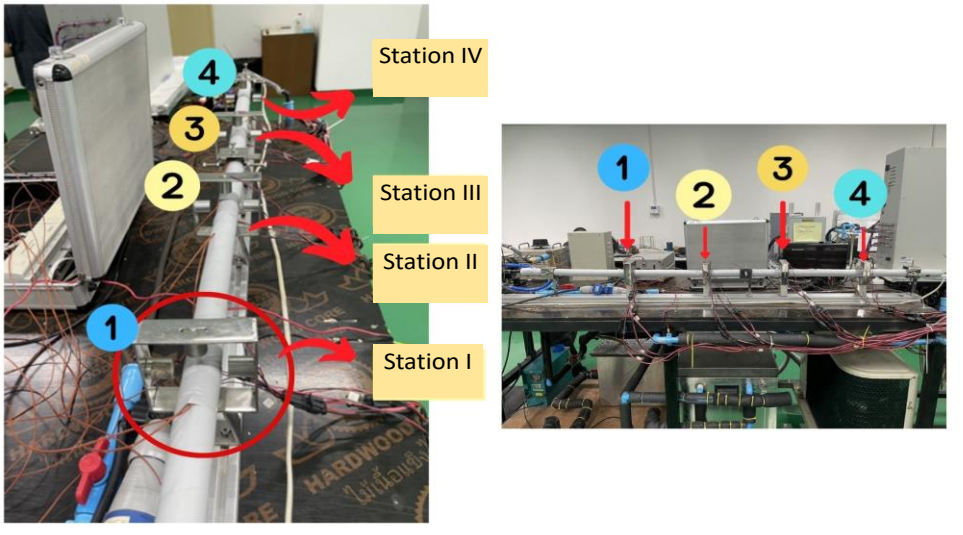

Fig. 2: Photograph of four electromagnetic field stations, in which each station has four units.

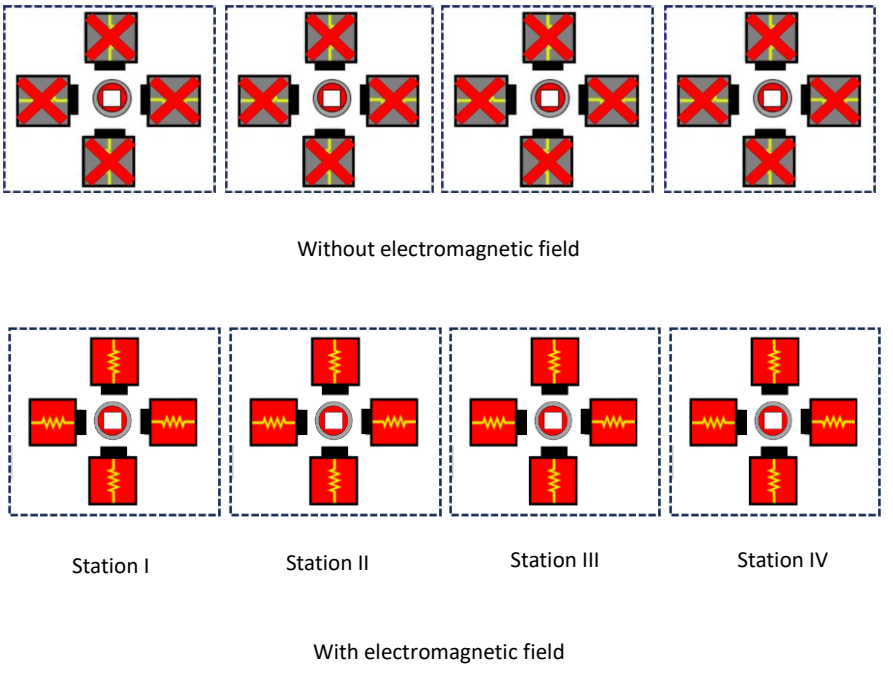

Fig. 3: The electromagnetic field unit working for turned off and turned on conditions.

2.4 The measured data reduction process and uncertainties analysis

Table 1 displays the magnetic particle and DI-water characteristics. The characteristics of ferrofluids are dictated by the suggested correlations (Equations 1-7) as follows: [38-41] Dynamic viscosity is given by Equation (1):[38]

$$\mu_{nf} = (1 + 2.5\varphi)\mu_w \tag{1}$$

Ferrofluid's density is given by Equation (2):[39]

$$\rho_{nf} = \varphi\rho_P + (1 - \varphi)\rho_w \tag{2}$$

Effective thermal conductivity is given by Equation (3):[40]

$$k_{nf} = \left[\frac{k_p+2k_w-2\varphi(k_w-k_p)}{k_p+2k_w+\varphi(k_w-k_p)}\right]k_w \tag{3}$$

Effective specific heat is given by Equation (4):[41]

$$(\rho C_p)_{nf} = \phi(\rho C_p)_p + (1 - \phi)(\rho C_p)_w \tag{4}$$

The Reynolds number (Re) is defined by Equation (5).

$$Re = \frac{\rho_{nf}V_\infty D_e}{\mu_{nf}} \tag{5}$$

Based on the heat transfer absorbed by a ferrofluid provided by an electric heater, the Nusselt number (Nu) is calculated by Equation (6).

$$Nu = \frac{hD_e}{k_{nf}} = \frac{[I\cdot Vol+(\rho A_{cr}V)_{nf}C_{p,nf}(T_{in,nf}-T_{out,nf})]/2}{\pi k_{nf}L(T_{wi,ave}-T_{nf,ave})} \tag{6}$$

The friction factor (f) may be obtained from Equation (7).

$$f = \frac{\Delta P}{\left(\frac{\rho_{nf}V_{nf}^2}{2}\right)\left(\frac{L}{D_e}\right)} \tag{7}$$

The Coleman and Steel technique calculates the uncertainty of measurement results.[42] The Nusselt number and friction factor in this research depend on several relevant factors, as seen by the equations above. The uncertainties may be computed using the instrument uncertainties by Equations (8) and (9) (Table 2).

$$\frac{\partial Nu}{Nu} = \sqrt{\begin{matrix}\left(\frac{\partial Nu}{V}\right)^2+\left(\frac{\partial Nu}{T_{wi,ave}}\right)^2+\left(\frac{\partial Nu}{T_{wo,ave}}\right)^2+\\ \left(\frac{\partial Nu}{T_{nf,ave}}\right)^2+\left(\frac{\partial Nu}{T_{in,nf}}\right)^2+\left(\frac{\partial Nu}{T_{out,nf}}\right)^2\end{matrix}} \tag{8}$$

$$\frac{\partial f}{f} = \sqrt{\left(\frac{\partial f}{V}\right)^2+\left(\frac{\partial f}{(\Delta P)}\right)^2} \tag{9}$$

The correctness of the Nusselt number and friction factor are ± 5.0 % and ± 4.5 %, respectively.

Table 2: Uncertainty and accuracy of the instruments.

Instruments	Accuracy	Uncertainty
Voltage supplied by power source, voltage	0.2%	±0.5
Current supplied by power source, ampere	0.2%	±0.5
Digital weight scale, gram	0.01%	±0.01
Thermocouple type T, Data logger, ^oC	0.1%	±0.1
Differential pressure transducer	0.02%	±0.02

3. Mathematical modeling

3.1 Physical model and equations

Fig. 4 depicts a tube with various configurations employed in the current investigation. Several important variables must be considered to achieve an optimal condition, including the design of the computational domain, grid configurations, and the computational method. Numerous connection types

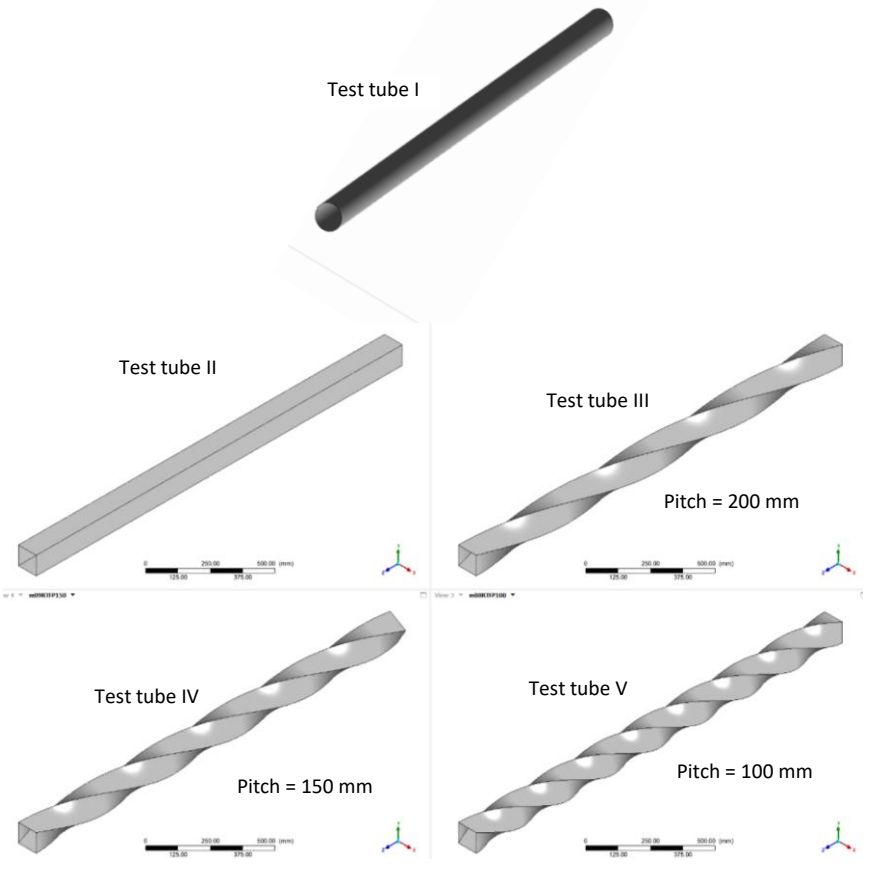

Fig. 4: Test section configuration in the present analysis.

between phases are studied in a two-phase model, in which the main Equations (10-14) for both phases are used:[43,44]

$$\nabla\left(\rho_l\phi_l\vec{V_l}\right)=0 \tag{10}$$

$$\nabla\left(\rho_p\phi_p\vec{V_p}\right)=0 \tag{11}$$

$$\phi_l+\phi_p=1 \tag{12}$$

$$\nabla\left(\rho_l\phi_l\vec{V_l}\vec{V_l}\right)=\phi_l\nabla p+\nabla\left(\phi_l\mu_l\left(\nabla\vec{V_l}+\nabla\vec{V_l}T\right)\right)$$

$$+F_d+F_{Vm} \tag{13}$$

$$\nabla\left(\rho_p\phi_p\vec{V_p}\vec{V_p}\right)=\phi_p\nabla p+\nabla\left(\phi_p\mu_p\left(\nabla\vec{V_p}+\nabla\vec{V_p}T\right)\right)-F_d+$$

$$F_{Vm}+F_{cd} \tag{14}$$

The energy equation (incompressible fluid and without viscous dissipation) can be presented as Equations (15) and (16):

$$\nabla\left(\rho_l\phi_lC_{p,l}T_l\vec{V_l}\right)=\nabla(\phi_lk_l\nabla T_l)-h_v\left(T_l-T_p\right) \tag{15}$$

$$\nabla\left(\rho_p\phi_pC_{p,p}T_p\vec{V_p}\right)=\nabla\left(\phi_pk_p\nabla T_p\right)-h_v\left(T_l-T_p\right) \tag{16}$$

3.2 Parameters definition

The virtual mass force grows in a direct proportion to the relative acceleration, as stated in a prior work in Equation (17).[45]

$$F_{vm}=\frac{0.5\phi_p\rho_lD\left(V_l-V_p\right)}{Dt} \tag{17}$$

The proposed correlation defines mutual contact force and modulus using Equations (18).[45]

$$F_{cd}=\phi_l\vec{\nabla}\phi_l\{exp(-600[\phi_l-0.376])\} \tag{18}$$

The drag force can be calculated by Equation (19):[45]

$$F_d=-\beta\left(\vec{V_l}-\vec{V_p}\right) \tag{19}$$

The friction coefficient can be determined from Equation (20):

$$\beta=\frac{3}{4}C_d\frac{\phi_l(1-\phi_l)}{d_p}\rho_l\left(\vec{V_l}-\vec{V_p}\right)\phi_l^{-265} \tag{20}$$

The drag coefficient is determined from Equations (21) and (22):

$$C_d=\begin{cases}\frac{24}{Re_p}\left(1+0.15Re_p^{0.687}\right),\ Re_p\langle 1000\\ 0.44,\ Re_p\rangle 1000\end{cases} \tag{21}$$

$$Re_p=\frac{\phi_l\rho_l|\vec{V_l}-\vec{V_p}|d_p}{\mu_l} \tag{22}$$

For mono-dispersed spherical particles, h_v can be determined from Equation (23), k_{bl} and k_{bp} are calculated in Equations (24-27):

$$h_v=\frac{6(1-\phi_l)}{d_p}\left(\left(2+1.1\,Re_p^{0.6}Pr^{1/3}\right)\frac{k_l}{d_p}\right) \tag{23}$$

$$k_{bl}=\left(1-\sqrt{(1-\phi_l)}\right)\frac{k_{bl}}{\phi_l} \tag{24}$$

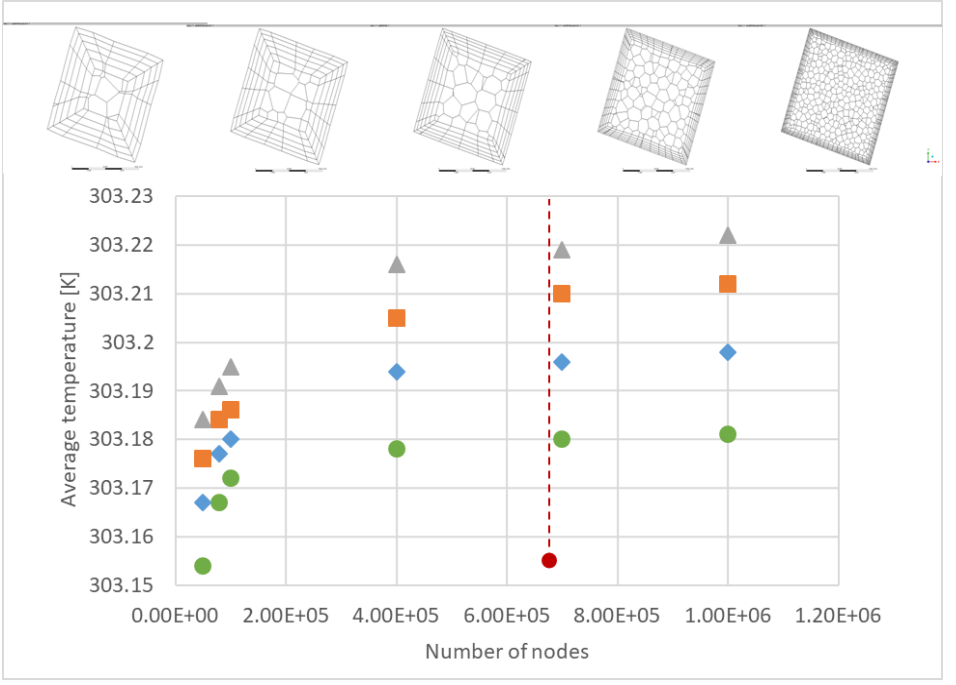

Fig. 5: Grid configuration for the numerical analysis and grid-independent test.

$$k_{bp} = \left(\sqrt{(1-\phi_l)}\right)\left(0.00726\frac{k_p}{k_l} + 0.99274\Gamma\right)\frac{k_{bl}}{\phi_l} \quad (25)$$

where

$$\Gamma = \frac{2}{\left(1-\frac{B}{A}\right)}\left\{\frac{B(A-1)}{A\left(1-\frac{B}{A}\right)^2}\right\} ln\left(\frac{A}{B}\right) - \frac{(B-1)}{\left(1-\frac{B}{A}\right)} - \frac{B+1}{2} \quad (26)$$

$$A = \frac{k_p}{k_l}, B = 1.25\left(\frac{1-\phi_l}{\phi_l}\right)^{10/9} \quad (27)$$

The effective thermal conductivities of each phase are obtained from Equations (28) and (29):

$$k_l = \frac{k_{bl}}{\phi_l} \quad (28)$$

$$k_p = \frac{k_{bp}}{\phi_p} \quad (29)$$

3.3 Numerical method and boundary conditions

The mathematical model was solved using the control volume technique (ANSYS FLUENT 16.2). The pressure-velocity coupling problem was addressed using a high-order discretization accuracy. Computers consisting of 18 cores and 96 GB RAM were used. It took around 35 hours to get the convergence results. The numerical procedures are conducted using the *Re* range of 4500 - 10,500. The simulation processes have the following boundary conditions:

- Outer wall: $q = q_{in}$
- Outlet: $P_{out} = P_{ambi}$
- Inner wall: no-slip condition
- Inlet: $T = T_{in}, V = V_{in}$

4. Results and discussion

4.1 Verification of the predicted results

Fig. 5 shows how a non-uniform mesh creates a finer mesh in the boundary layer zone. The grid independence verification in the computational approach is done on various grid sizes. Fig. 5 also shows how the number of nodes varies from 400,000 to 1,000,000. The average coolant temperature varies with the nodes, and the difference in outlet temperatures between node numbers 600,000 and 1,000,000 is less than 1%. This demonstrates that the outcomes are independent of node values larger than 600,000. As a result, the numerical method produces adequate results with a node number of 600,000. Furthermore, the residual parameter has a convergence criterion of fewer than 10^{-6}. The findings from the present numerical model were compared to experimental data in a twisted square tube to validate the numerical technique. The boundary conditions for numerical calculations were determined, and the average outflow ferrofluid temperatures were calculated. Table 3 shows the comparison of the output temperatures. The greatest difference between predicted results and measured data was found to be 7.92%.

4.2 Verification of the measured results

This study looks at the heat-removal capabilities of magnetic fluid in a square tube under fixed and pulsing EFs. The current study is verified to confirm the reproducibility of the experimental setting. It is revealed that no previously published data under comparable conditions exist to substantiate the cited conclusions. The measured data may be confirmed by comparing them to tubes with different designs. The square tube results are checked against previously published data for the Nusselt number and for the friction factor. Fig. 6(A) plots the Nusselt number values from the measured data against the published findings. The reported Nusselt number errors are 17.31, 11.88, and 10.47%,

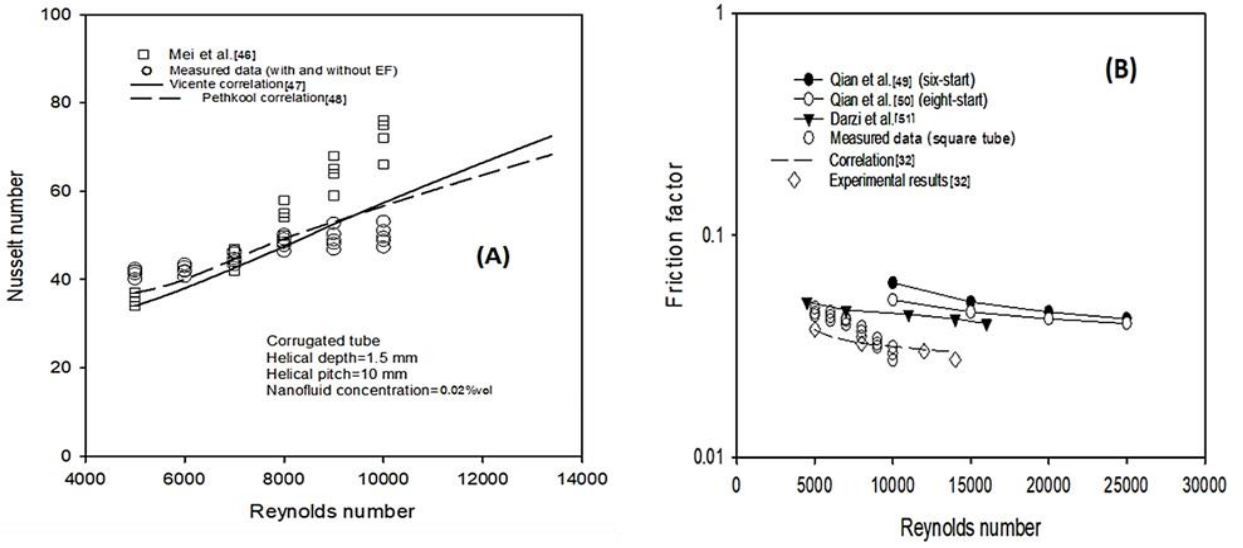

Fig. 6: Comparison of the measured data with the published results: (A) Nusselt number values and (B) friction factor.

Table 3: Comparison between the predicted results and the measured data.

Tubes	Coolants	Outlet coolant temperature (°C)		
		Measured data	Predicted results	Error (%)
Straight circular tube	Water	21.23	22.55	6.03
Straight square tube	Water	21.56	23.17	7.21
Twisted square tube with pitch=200 mm	Ferrofluid	21.87	23.54	7.36
Twisted square tube with pitch=100 mm	Ferrofluid	22.32	24.16	7.92

respectively.[46-48] Fig. 6(B) plots the published data against the observed flow resistance values.[49-51,32] The reported data in Ref. [49-51,32] with accuracy values of 25.91, 18.69, 13.00 and 11.32%, respectively. The construction method may impact the corrugation form, angle, tube configurations, and operating conditions, all of which are essential elements in this capacity ability to remove heat and withstand flow. One of the most probable sources of disagreement might be the manufacturing process, which has multiple configurations.

4.3 Effect of the twisted pitch

Fig. 7(A) displays the Nusselt number at different twisted pitch distances without an EF. Increased flow disturbance considerably improves turbulent intensity and nanoparticle mixing levels. Consequently, the twisted square tube obtains a greater heat transfer coefficient with a shorter twisted pitch distance. The average Nusselt number rose by 5.45, 8.54, and 12.54 % for twisted pitch distances of 100, 150, and 200 mm, respectively. Fig. 7(B) demonstrates the impact of the twisted pitch distances on the flow friction factor. As the flow rate increases, the twisted roughness migrates to the laminar sublayer and becomes sensitive to the core flow. The normal stress grows as the Reynolds number climbs, whereas shear stress declines near wall surfaces. Furthermore, disruption in this layer significantly affects the flow turbulence. As a consequence, the twisted tube surface has a substantial influence on the flow friction factor. Twisted pitches of 100, 150, and 200 mm increase friction factor by 4.345, 7.86, and 12.32%, respectively, compared to straight square tubes.

4.4 Effect of coolant types

Fig. 8 shows how the Nusselt number and friction factor vary for two coolants in a twisted square tube without an EF. Flowing in the twisted tube induces varying fluid transport qualities and secondary and swirling flows. Nanoparticles increase thermal conductivity and cause nanoparticles to move in a Brownian way. As a result, employing nanofluids as the coolant produces a greater Nusselt number than using water, about 7.89%. However, the presence of nanoparticles has two substantial impacts on its thermal and hydraulic properties. Higher thermal conductivity results in increasing heat removal ability. For an unwanted consequence, nanofluids dynamic viscosity and density increase, resulting in a larger pressure drop. However, employing nanofluids as a coolant has a greater friction factor than water and tends to grow with increased power input.

4.5 Effect of an electromagnetic flux

Fig. 9 depicts the Nusselt number and friction factor for different electromagnetic fluxes. The Nusselt number is larger with EF than that without it. This is due to the EF impact on the migration of suspended particles toward the twisted square tube wall. Nanoparticles continue to move toward the wall due to the EF. It considerably impacts the boundary layer

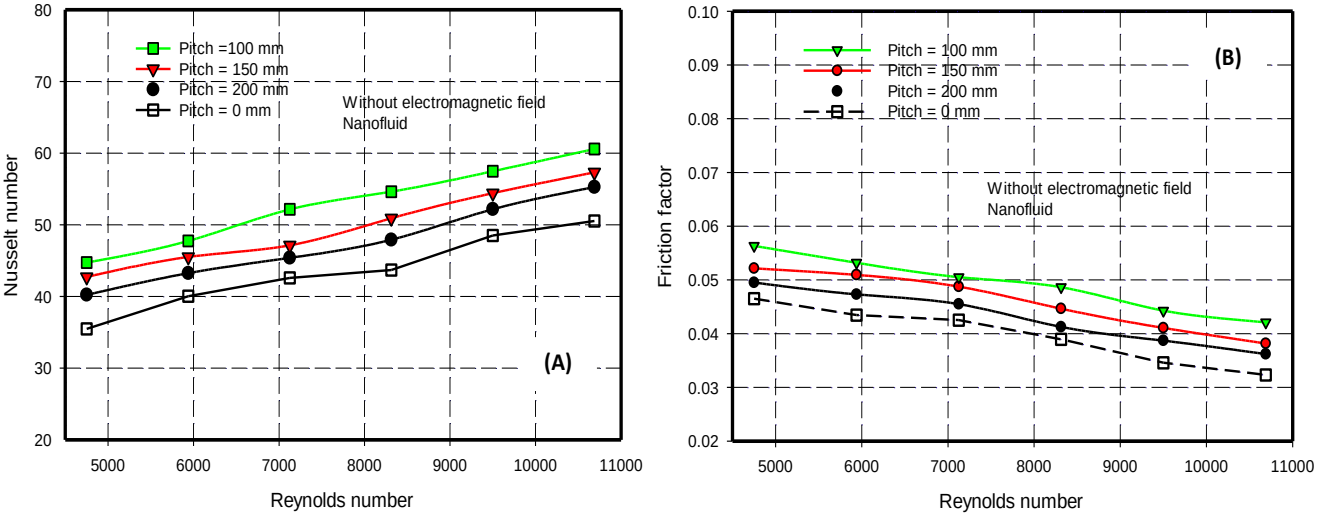

Fig. 7: Variation of (A) Nusselt number and (B) friction factor with a different twisted pitch without electromagnetic field.

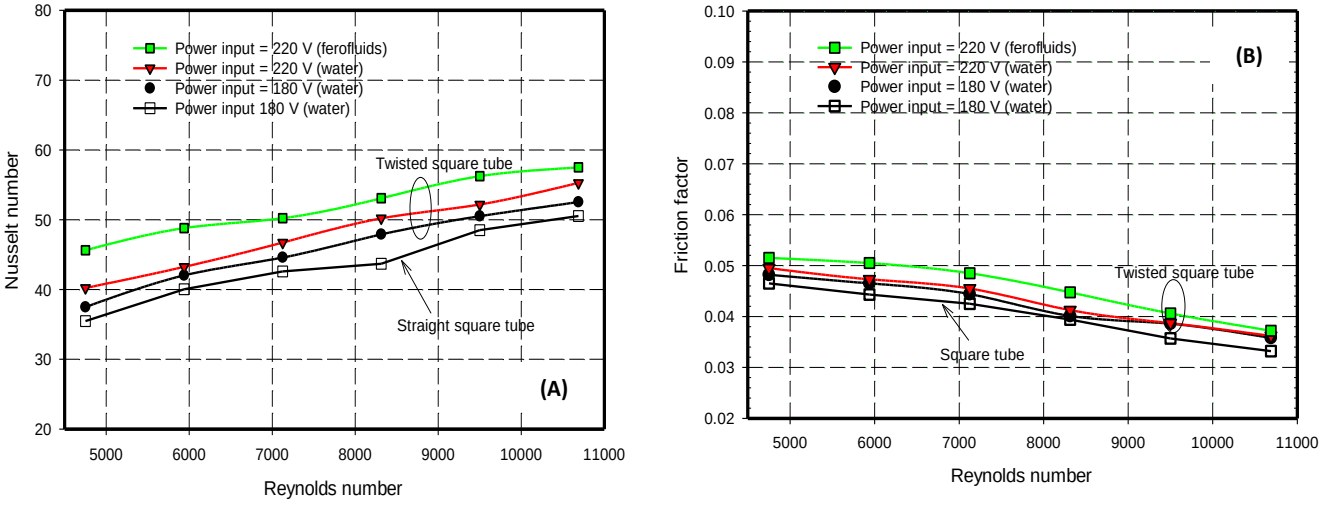

Fig. 8: Variation of (A) Nusselt number and (B) friction factor with a different power input of the twisted square tube (pitch = 150 mm) without electromagnetic field.

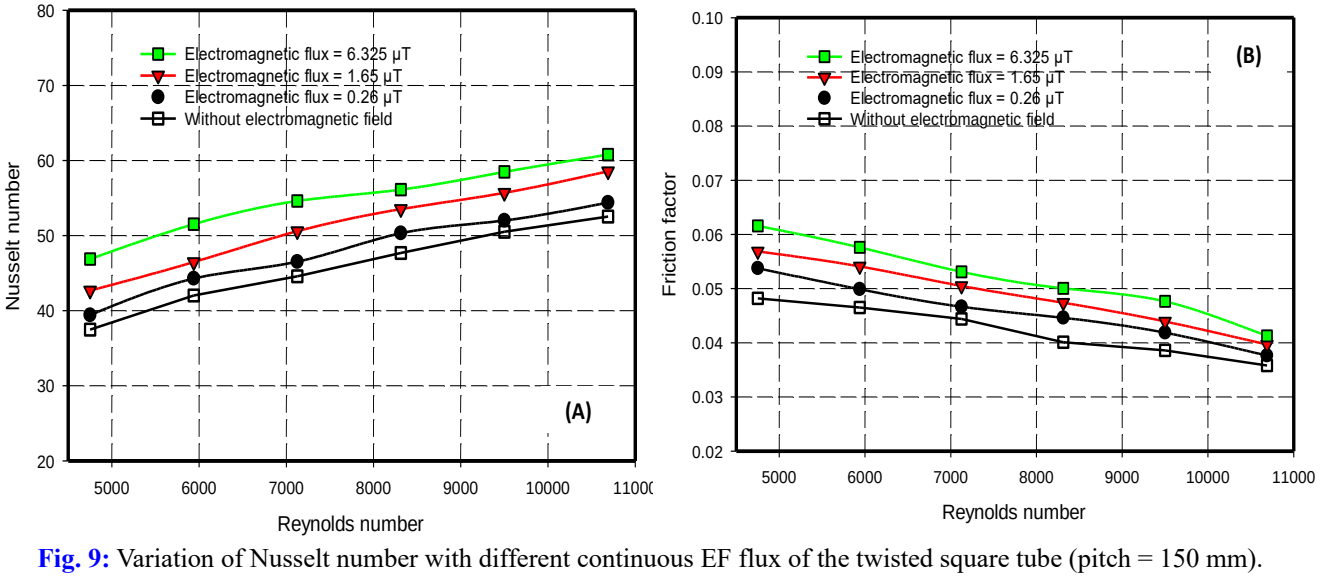

Fig. 9: Variation of Nusselt number with different continuous EF flux of the twisted square tube (pitch = 150 mm).

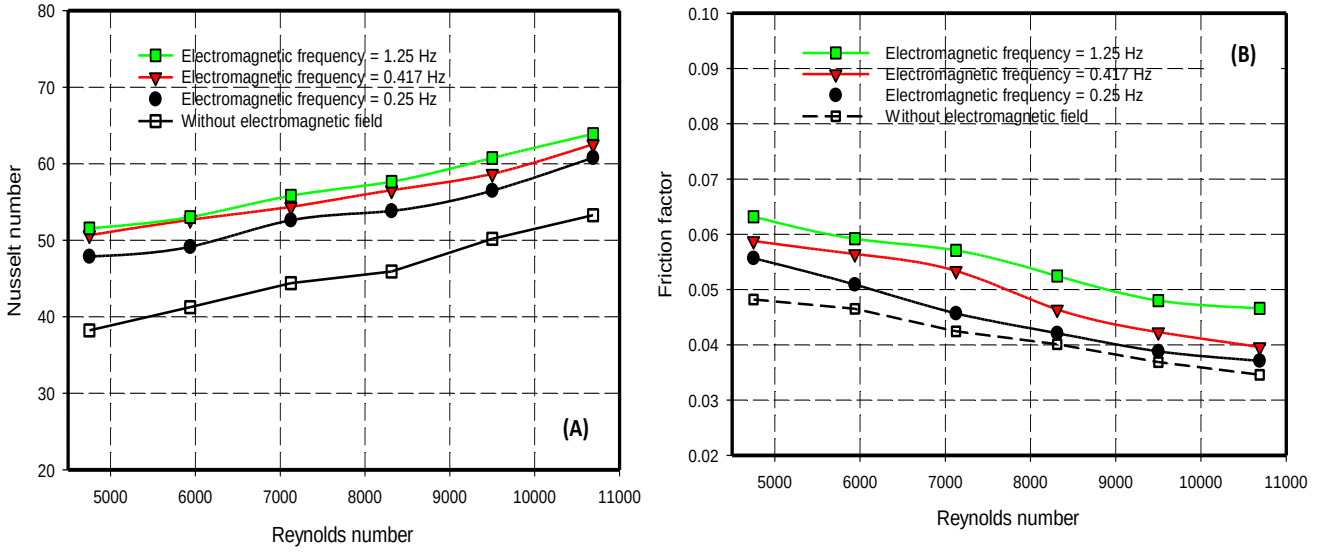

Fig. 10: Variation of (A) Nusselt number and (B) friction factor with different EF frequency of the twisted square tube (pitch = 150 mm) at continuous EF flux 6.25 μT.

disturbance during operation, resulting in greater heat removal capacities. Furthermore, increased electromagnetic flux improves nanoparticle mixing and local thermal conductivity. The Nusselt number rises by 4.65, 8.23, and 13.76% for electromagnetic fluxes of 0.25, 1.56, and 6.33 μT, respectively. A higher electromagnetic flux causes a more considerable mixing of nanoparticles along the square tube wall, resulting in flow resistance. As seen in Fig. 9, the friction factor increases as the electromagnetic flux rises.

4.6 Effect of an electromagnetic frequency

Without the EF effect, the main flow and flow closed the wall travel along the square tube length; the turbulence intensity and mixing level determine the coolant flow velocity. As a consequence, the suspended nanoparticles travel in the same direction as the base fluid throughout the square tube length. The EF effect produces an induced force in the transverse direction. This force influences the nanoparticles migration direction, which is toward the square tube wall. Migrating nanoparticles to the wall causes higher mixing levels, boundary layer disturbance, and local thermal conductivity. These phenomena contribute to thermal cooling capabilities. The Nusselt value that includes the EF effect is larger than the one without it. The intensity of turbulent flow created by the EF effect, on the other hand, is proportional to the induced force. The suspended nanoparticles move rhythmically in response to the oscillation frequency of EF, resulting in increased mixing turbulence intensity and a higher value as the oscillation frequency increases. Therefore. As demonstrated in Fig. 10, the Nusselt number and friction factor rise as the electromagnetic frequency increases. The rotational direction frequency has a considerable impact on nanoparticle mobility. This causes a greater fluid velocity along the tube wall and a higher mixing level and turbulence intensity, which causes the friction factor to vary.

4.7 Temperature and flow behaviors

Fig. 11 depicts temperature distributions along a tube with various tube shapes. The numerical procedure was carried out using a circular diameter and a square tube width×height of 10 mm and 10×10 mm, respectively, using the identical constant heat power input. The circular tube has the highest tube temperatures of the square tubes due to the boundary layer disruption and the less surface area, which results in more heat removal. Furthermore, the greatest tube temperature in a twisted square tube is lower than that in a straight square tube, and it decreases with increasing twisted pitch distance. The vorticity flow occurs at the square tube four dead corners. As a result, this location has the greatest temperature. For the straight square tube, the core flow and the flow in the boundary layer zone travel along the tube length—the turbulence intensity and mixing level determine the flow velocity of the coolant. Consequently, the suspended nanoparticles travel in the same direction as the base fluid along the square tube.

In contrast, with the twisted square tube, the ferrofluid in the boundary layer zone flows along the twisted wall direction. This flow behavior influences the direction of movement of the nanoparticles, increases mixing levels, and disrupts the boundary layer, as shown in Fig. 12. This behavior provides greater heat removal capacity than the straight square tube. Figs. 13-15 show the temperature distribution, streamlines, and vorticity vectors at various cross-section planes of three analyzed twisted pitch distance tubes without the impact of MF. The vorticity of the twisted square tube is more than that of the straight square tube. Furthermore, these data show that the vorticity increases toward the wall, notably in the twisted square tube. Less twisted pitch causes greater vorticity intensification. Furthermore, increasing the *Re* has a greater impact on intensifying vorticity in the twisted square tube. Intensifying flow rate with MF may improve flow mixing and raise Δp within twisted square tubes.

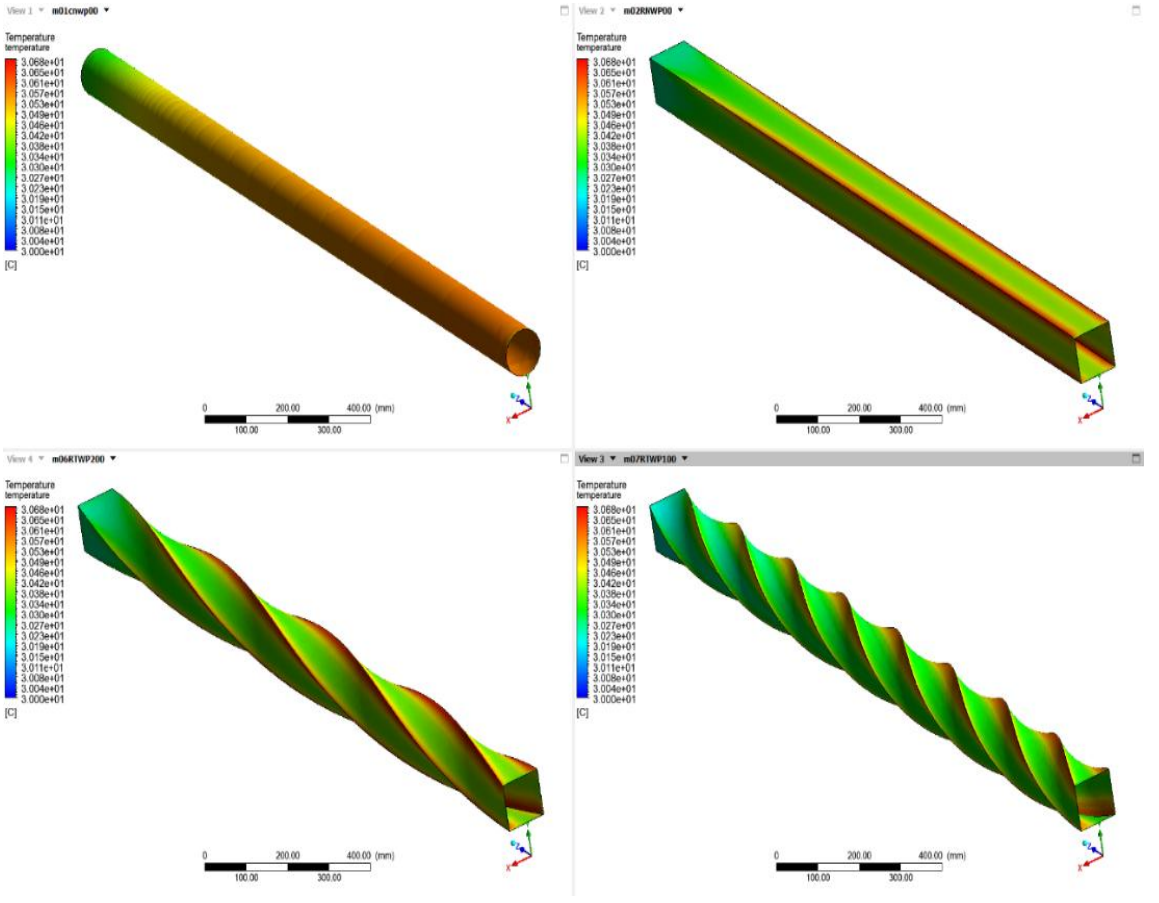

Fig. 11: The temperature distribution of the twisted square tube with different pitches for ferrofluid at inlet temperature = 30 ºC.

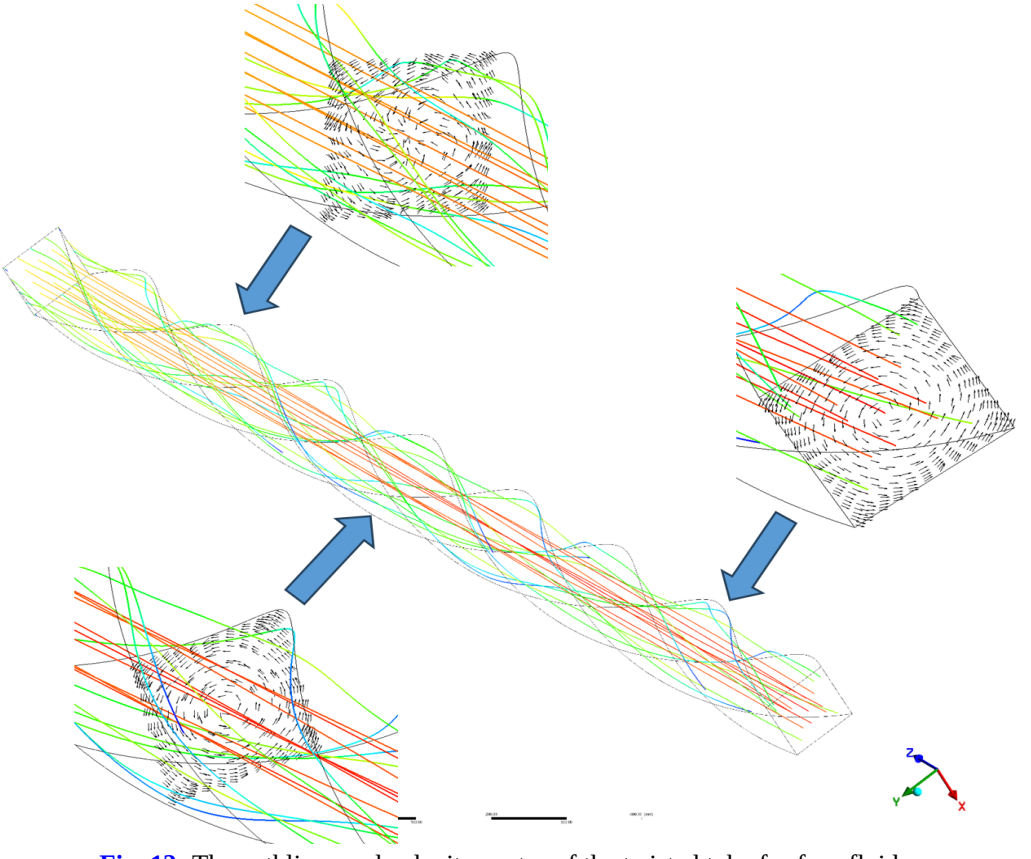

Fig. 12: The pathlines and velocity vector of the twisted tube for ferrofluid.

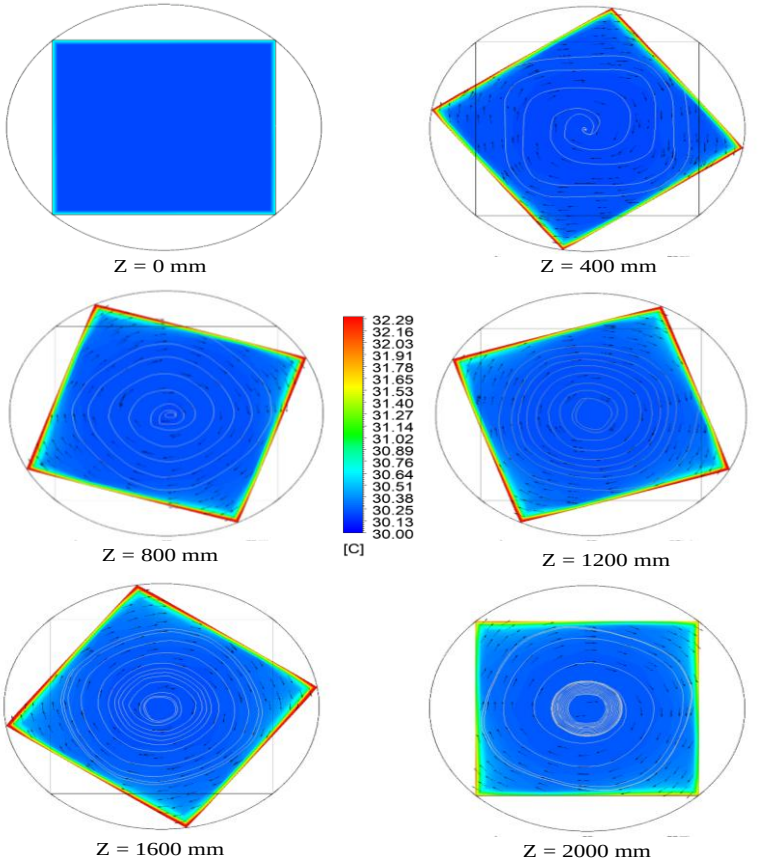

Fig. 13: The temperature distribution, streamlines, and velocity vector of the twisted tube with pitch = 100 mm for ferrofluid at inlet temperature = 30 ^{o}C.

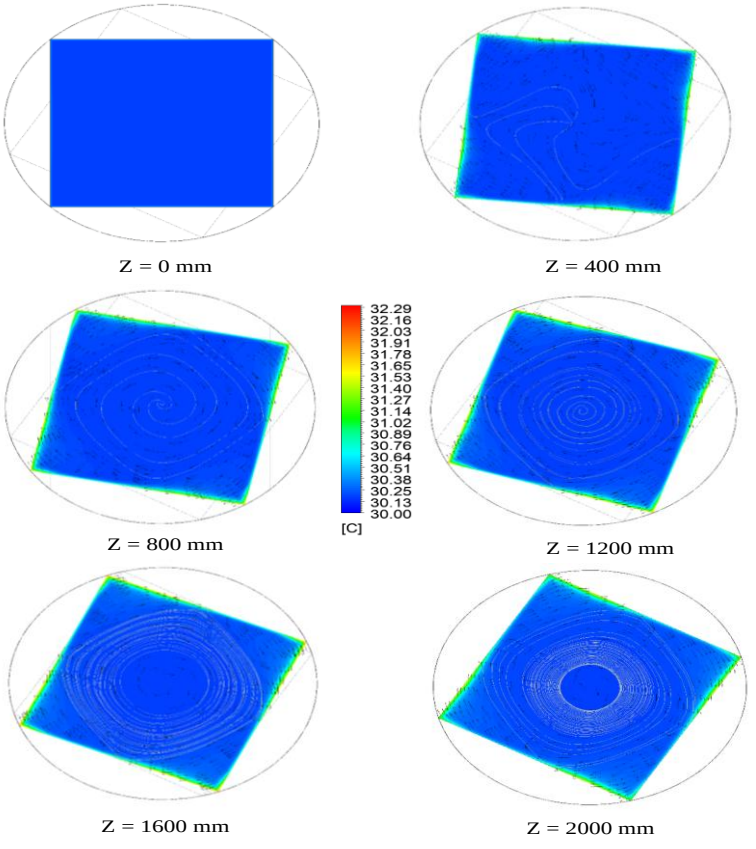

Fig. 14: The temperature distribution, streamlines, and velocity vector of the twisted tube with pitch = 150 mm for ferrofluid at inlet temperature = 30 ^{o}C.

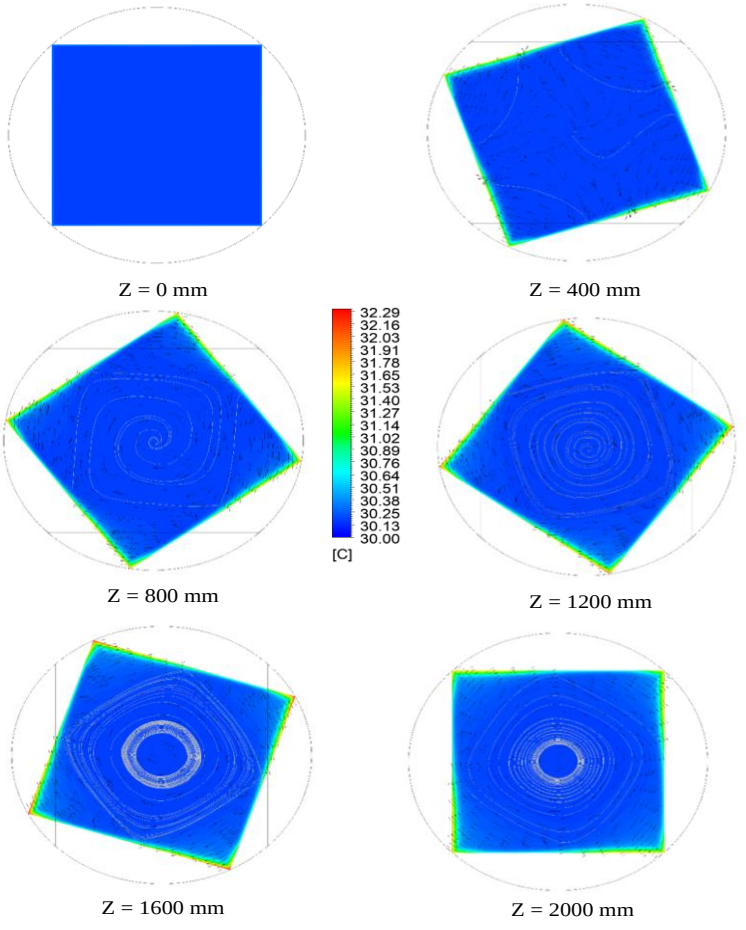

Fig. 15: The temperature distribution, streamlines, and velocity vector along the twisted square tube with pitch = 200 mm for ferrofluid at inlet temperature = 30 ºC.

5. Conclusion

This research investigated magnetic fluid flow heat and flow behaviors within twisted square tubes with varying twisted pitches, with and without an EF influence. Without EF, the twisted square tube has a higher Nusselt number (4.58-10.50%) and friction factor (4.12-8.7%) than the straight square tube. Compared to water, the magnetic fluid Nusselt number and friction factor increased by 10.5 and 5.35%, respectively. The EF causes particles to travel to the square tube wall, which significantly affects the boundary layer disturbance. The EF flux effect increases the Nusselt number and friction factor by 10.71 and 5.78%, respectively. In addition to the EF frequency effect, the Nusselt number rises by 13.45%, while the friction factor increases by 12.76%. Furthermore, the projected findings are quite consistent with the observed data and in high agreement with the published results.

Nomenclature

A area, [m^2]
C_p specific heat, [$kJkg^{-1}$ $^oC^{-1}$]
D diameter, [m]
f friction factor, [-]
h heat transfer coefficient, [kWm^{-2} $^oC^{-1}$]
I electrical current, [A]
k thermal conductivity, [kWm^{-1} $^oC^{-1}$]
L tube length, [m]
Nu Nusselt number, [-]
P pressure, [kNm^{-2}]
Re Reynolds number, [-]
T temperature, [^oC]
V velocity, [ms^{-1}]
Vol voltage, [V]
W width, [cm]

Greek symbol

φ nanofluids concentration, [%vol.]
ρ density, [kgm^{-3}]
μ viscosity, [$kg\ m^{-1}s^{-1}$]

Subscripts

cr *cross-section*
e equivalent
in inlet
l liquid
nf nanofluids
p particles
w water

Acknowledgments

The authors thank Srinakharinwirot University (SWU) Faculty of Engineering for their financial help with this work.

Conflict of Interest

There is no conflict of interest.

Supporting Information

Not applicable.

References

[1] R. Ganguly, S. Sen, I. K. Puri, Heat transfer augmentation using a magnetic fluid under the influence of a line dipole, *Journal of Magnetism and Magnetic Materials*, 2004, **271**, 63-73, doi: 10.1016/j.jmmm.2003.09.015.

[2] P. Naphon, L. Nakharintr, Turbulent two phase approach model for the nanofluids heat transfer analysis flowing through the minichannel heat sinks, *International Journal of Heat and Mass Transfer*, 2015, **82**, 388-395, doi: 10.1016/j.ijheatmasstransfer.2014.11.024.

[3] L. Nakharintr, P. Naphon, S. Wiriyasart, Effect of jet-plate spacing to jet diameter ratios on nanofluids heat transfer in a mini-channel heat sink, *International Journal of Heat and Mass Transfer*, 2018, **116**, 352-361, doi: 10.1016/j.ijheatmasstransfer.2017.09.037.

[4] P. Naphon, S. Wiriyasart, T. Arisariyawong, T. Nualboonrueng, Magnetic field effect on the nanofluids convective heat transfer and pressure drop in the spirally coiled tubes, *International Journal of Heat and Mass Transfer*, 2017, **110**, 739-745, doi: 10.1016/j.ijheatmasstransfer.2017.03.077.

[5] P. Naphon, S. Wiriyasart, T. Arisariyawong, Artificial neural network analysis the pulsating Nusselt number and friction factor of TiO_2/water nanofluids in the spirally coiled tube with magnetic field, *International Journal of Heat and Mass Transfer*, 2018, **118**, 1152-1159, doi: 10.1016/j.ijheatmasstransfer.2017.11.091.

[6] P. Naphon, S. Wiriyasart, T. Arisariyawong, L. Nakharintr, ANN, numerical and experimental analysis on the jet impingement nanofluids flow and heat transfer characteristics in the micro-channel heat sink, *International Journal of Heat and Mass Transfer*, 2019, **131**, 329-340, doi: 10.1016/j.ijheatmasstransfer.2018.11.073.

[7] A. Siricharoenpanitch, S. Wiriyasart, P. Vengsungnle, N. Naphon, P. Naphon, Heat transfer and flow behaviors of ferrofluid in three-start helically fluted tubes, *Heat Transfer Engineering*, 2022, **43**, 1769-1782, doi: 10.1080/01457632.2021.2009227.

[8] Q. Li, Y. Xuan, Experimental investigation on heat transfer characteristics of magnetic fluid flow around a fine wire under the influence of an external magnetic field, *Experimental Thermal and Fluid Science*, 2009, **33**, 591-596, doi: 10.1016/j.expthermflusci.2008.12.003.

[9] Y. Iwamoto, H. Yamaguchi, X. D. Niu, Magnetically-driven heat transport device using a binary temperature-sensitive magnetic fluid, *Journal of Magnetism and Magnetic Materials*, 2011, **323**, 1378-1383, doi: 10.1016/j.jmmm.2010.11.050.

[10] H. Salehi, S. Zeinali Heris, F. Sharifi, M. A. Razbani, Effects of a nanofluid and magnetic field on the thermal efficiency of a two-phase closed thermosyphon, *Heat Transfer—Asian Research*, 2013, **42**, 630-650, doi: 10.1002/htj.21043.

[11] E. Chiavazzo, M. Fasano, P. Asinari, P. Decuzzi, Scaling behaviour for the water transport in nanoconfined geometries, *Nature Communications*, 2014, **5**, 3565, doi: 10.1038/ncomms4565.

[12] G. Ibáñez, S. Cuevas, M. López de Haro, Optimization of a magnetohydrodynamic flow based on the entropy generation minimization method, *International Communications in Heat and Mass Transfer*, 2006, **33**, 295-301, doi: 10.1016/j.icheatmasstransfer.2005.12.003.

[13] C. Tangthieng, B. A. Finlayson, J. Maulbetsch, T. Cader, Heat transfer enhancement in ferrofluids subjected to steady magnetic fields, *Journal of Magnetism and Magnetic Materials*, 1999, **201**, 252-255, doi: 10.1016/S0304-8853(99)00062-1.

[14] E. E. Tzirtzilakis, V. D. Sakalis, N. G. Kafoussias, P. M. Hatzikonstantinou, Biomagnetic fluid flow in a 3D rectangular duct, *International Journal for Numerical Methods in Fluids*, 2004, **44**, 1279-1298, doi: 10.1002/fld.618.

[15] A. Jafari, T. Tynjälä, S. M. Mousavi, P. Sarkomaa, Simulation of heat transfer in a ferrofluid using computational fluid dynamics technique, *International Journal of Heat and Fluid Flow*, 2008, **29**, 1197-1202, doi: 10.1016/j.ijheatfluidflow.2008.01.007.

[16] H. Aminfar, M. Mohammadpourfard, S. Ahangar Zonouzi, Numerical study of the ferrofluid flow and heat transfer through a rectangular duct in the presence of a non-uniform transverse magnetic field, *Journal of Magnetism and Magnetic Materials*, 2013, **327**, 31-42, doi: 10.1016/j.jmmm.2012.09.011.

[17] M. Afrand, S. Farahat, A. H. Nezhad, G. Ali Sheikhzadeh, F. Sarhaddi, S. Wongwises, Multi-objective optimization of natural convection in a cylindrical annulus mold under magnetic field using particle swarm algorithm, *International Communications in Heat and Mass Transfer*, 2015, **60**, 13-20, doi: 10.1016/j.icheatmasstransfer.2014.11.006.

[18] M. Lajvardi, J. Moghimi-Rad, I. Hadi, A. Gavili, T. Dallali Isfahani, F. Zabihi, J. Sabbaghzadeh, Experimental investigation for enhanced ferrofluid heat transfer under magnetic field effect, *Journal of Magnetism and Magnetic Materials*, 2010, **322**, 3508-3513, doi: 10.1016/j.jmmm.2010.06.054.

[19] A. Malvandi, M. R. Safaei, M. H. Kaffash, D. D. Ganji, MHD mixed convection in a vertical annulus filled with Al_2O_3-water nanofluid considering nanoparticle migration, *Journal of Magnetism and Magnetic Materials*, 2015, **382**, 296-306, doi: 10.1016/j.jmmm.2015.01.060.

[20] O. Mahian, S. Mahmud, I. Pop, Analysis of first and second laws of thermodynamics between two isothermal cylinders with relative rotation in the presence of MHD flow, *International Journal of Heat and Mass Transfer*, 2012, **55**, 4808-4816, doi: 10.1016/j.ijheatmasstransfer.2012.04.048.

[21] A. Ghofrani, M. H. Dibaei, A. Hakim Sima, M. B. Shafii, Experimental investigation on laminar forced convection heat transfer of ferrofluids under an alternating magnetic field, *Experimental Thermal and Fluid Science*, 2013, **49**, 193-200, doi: 10.1016/j.expthermflusci.2013.04.018.

[22] M. M. Rashidi, N. Kavyani, S. Abelman, Investigation of entropy generation in MHD and slip flow over a rotating porous disk with variable properties, *International Journal of Heat and Mass Transfer*, 2014, **70**, 892-917, doi: 10.1016/j.ijheatmasstransfer.2013.11.058.

[23] S. Mojumder, K. M. Rabbi, S. Saha, M. Hasan, S. C. Saha, Magnetic field effect on natural convection and entropy generation in a half-moon shaped cavity with semi-circular

bottom heater having different ferrofluid inside, *Journal of Magnetism and Magnetic Materials*, 2016, **407**, 412-424, doi: 10.1016/j.jmmm.2016.01.046.
[24] L. Sha, Y. Ju, H. Zhang, The influence of the magnetic field on the convective heat transfer characteristics of Fe_3O_4/water nanofluids, *Applied Thermal Engineering*, 2017, **126**, 108-116, doi: 10.1016/j.applthermaleng.2017.07.150.
[25] N. Gan Jia Gui, C. Stanley, N. T. Nguyen, G. Rosengarten, Ferrofluids for heat transfer enhancement under an external magnetic field, *International Journal of Heat and Mass Transfer*, 2018, **123**, 110-121, doi: 10.1016/j.ijheatmasstransfer.2018.02.100.
[26] L. Shi, Y. He, Y. Hu, X. Wang, Thermophysical properties of Fe_3O_4@CNT nanofluid and controllable heat transfer performance under magnetic field, *Energy Conversion and Management*, 2018, **177**, 249-257, doi: 10.1016/j.enconman.2018.09.046.
[27] P. Naphon, S. Wiriyasart, Pulsating flow and magnetic field effects on the convective heat transfer of TiO_2-water nanofluids in helically corrugated tube, *International Journal of Heat and Mass Transfer*, 2018, **125**, 1054-1060, doi: 10.1016/j.ijheatmasstransfer.2018.05.015.
[28] S. W. Han, H. J. Cho, S. Y. Jin, M. Sedén, I. B. Lee, I. Sohn, Effects of simultaneous static and traveling magnetic fields on the molten steel flow in a continuous casting mold, *Metallurgical and Materials Transactions B*, 2018, **49**, 2757-2769, doi: 10.1007/s11663-018-1356-y.
[29] C. Yang, G. Liu, J. Zhang, J. Qian, Thermohydraulic analysis of hybrid smooth and spirally corrugated tubes, *International Journal of Thermal Sciences*, 2020, **158**, 106520, doi: 10.1016/j.ijthermalsci.2020.106520.
[30] P. Naphon, T. Arisariyawong, S. Wiriyasart, A. Srichat, ANFIS for analysis friction factor and Nusselt number of pulsating nanofluids flow in the fluted tube under magnetic field, *Case Studies in Thermal Engineering*, 2020, **18**, 100605, doi: 10.1016/j.csite.2020.100605.
[31] T. Zhang, D. Che, Y. Zhu, H. Shi, D. Chen, Effects of magnetic field and inclination on natural convection in a cavity filled with nanofluids by a double multiple-relaxation-time thermal lattice Boltzmann method, *Heat Transfer Engineering*, 2020, **41**, 252-270, doi: 10.1080/01457632.2018.1528057.
[32] A. Siricharoenpanitch, S. Wiriyasart, P. Vengsungnle, N. Naphon, P. Naphon, Heat transfer of ferrofluid in fluted tubes with an electromagnetic field, *Heat Transfer Engineering*, 2023, **44**, 426-441, doi: 10.1080/01457632.2022.2068219.
[33] M. Gürdal, K. Arslan, E. Gedik, A. A. Minea, Effects of using nanofluid, applying a magnetic field, and placing turbulators in channels on the convective heat transfer: A comprehensive review, *Renewable and Sustainable Energy Reviews*, 2022, **162**, 112453, doi: 10.1016/j.rser.2022.112453.
[34] F. Fan, C. Qi, Q. Liu, M. Sheikholeslami, Effect of twisted turbulator perforated ratio on thermal and hydraulic performance of magnetic nanofluids in a novel thermal exchanger system, *Case Studies in Thermal Engineering*, 2020, **22**, 100761, doi: 10.1016/j.csite.2020.100761.
[35] S. Arunkumar H., S. Kumar, K. V. Karanth, A numerical study on the performance of different shaped perforation hole on the absorber duct insert in a solar air heater, *Engineered Science*, 2022, **18**, 234-242, doi: 10.30919/es8d644.
[36] A. S. El-Shafay, A. M. Mohamed, Ü. Ağbulut, M. S. Gad, Investigation of the effect of magnetic field on the PEC and exergy of heat exchanger filled with two-phase hybrid nanofluid, equipped with an edged twisted tape, *Engineering Analysis with Boundary Elements*, 2023, **148**, 153-164, doi: 10.1016/j.enganabound.2022.12.025.
[37] P. Vengsungnle, J. Jongpleampiti, N. Naphon, S. Poojeera, A. Srichat, S. Eiamsa-ard, P. Naphon, Oscillating electromagnetic field effect on nusselt number and pressure drop of ferrofluid in the fluted tubes, *Engineered Science*, 2024, **32**, 1307, doi:10.30919/es1307.
[38] B. C. Pak, Y. I. Cho, Hydrodynamic and heat transfer study of dispersed fluids with submicron metallic oxide particles, *Experimental Heat Transfer*, 1998, **11**, 151-170, doi: 10.1080/08916159808946559.
[39] Y. Xuan, W. Roetzel, Conceptions for heat transfer correlation of nanofluids, *International Journal of Heat and Mass Transfer*, 2000, **43**, 3701-3707, doi: 10.1016/s0017-9310(99)00369-5.
[40] D. A. Drew, S. L. Passman, Theory of multicomponent fluids, New York, Springer New York, 1999, ISBN: 101468492276.
[41] J. C. Maxwell, A treatise on electricity and magnetism, Cambridge, UK, Cambridge University Press, 2010, ISBN: 100486606368.
[42] H. W. Coleman, W. G. Steele, Experimental and uncertainty analysis for engineers, John Wiley & Sons, New York, 1989, ISBN: 100471121460.
[43] M. Akbari, N. Galanis, A. Behzadmehr, Comparative analysis of single and two-phase models for CFD studies of nanofluid heat transfer, *International Journal of Thermal Sciences*, 2011, **50**, 1343-1354, doi: 10.1016/j.ijthermalsci.2011.03.008.
[44] M. Kalteh, A. Abbassi, M. Saffar-Avval, A. Frijns, A. Darhuber, J. Harting, Experimental and numerical investigation of nanofluid forced convection inside a wide microchannel heat sink, *Applied Thermal Engineering*, 2012, **36**, 260-268, doi: 10.1016/j.applthermaleng.2011.10.023.
[45] M. Kalteh, A. Abbassi, M. Saffar-Avval, J. Harting, Eulerian–Eulerian two-phase numerical simulation of nanofluid laminar forced convection in a microchannel, *International Journal of Heat and Fluid Flow*, 2011, **32**, 107-116, doi: 10.1016/j.ijheatfluidflow.2010.08.001.
[46] S. Mei, C. Qi, T. Luo, X. Zhai, Y. Yan, Effects of magnetic field on thermo-hydraulic performance of Fe_3O_4-water nanofluids in a corrugated tube, *International Journal of Heat and Mass Transfer*, 2019, **128**, 24-45, doi: 10.1016/j.ijheatmasstransfer.2018.08.071.
[47] P. G. Vicente, A. García, A. Viedma, Experimental investigation on heat transfer and frictional characteristics of spirally corrugated tubes in turbulent flow at different Prandtl numbers, *International Journal of Heat and Mass Transfer*, 2004,

47, 671-681, doi: 10.1016/j.ijheatmasstransfer.2003.08.005.
[48] S. Pethkool, S. Eiamsa-ard, S. Kwankaomeng, P. Promvonge, Turbulent heat transfer enhancement in a heat exchanger using helically corrugated tube, *International Communications in Heat and Mass Transfer*, 2011, **38**, 340-347, doi: 10.1016/j.icheatmasstransfer.2010.11.014.
[49] J. Qian, C. Yang, Z. Wu, X. Liu, X. Gao, Z. Jin, B. Sunden, Analysis of fouling in six-start spirally corrugated tubes, *Heat Transfer Engineering*, 2020, **41**, 1885-1900, doi: 10.1080/01457632.2019.1675246.
[50] J. Qian, C. Yang, M. Chen, Z. Jin, Thermohydraulic performance evaluation of multi-start spirally corrugated tubes, *International Journal of Heat and Mass Transfer*, 2020, **156**, 119876, doi: 10.1016/j.ijheatmasstransfer.2020.119876.
[51] A. A. R. Darzi, M. Farhadi, K. Sedighi, Experimental investigation of convective heat transfer and friction factor of Al2o3/water nanofluid in helically corrugated tube, *Experimental Thermal and Fluid Science*, 2014, **57**, 188-199, doi: 10.1016/j.expthermflusci.2014.04.024.